謝　辞

本稿の執筆および拡散テンソル画像の研究にあたっては、以下の諸先生方の貴重なご指導・ご協力を賜りましたので、この場をお借りして厚く御礼申し上げます(敬称略)。

森　進・山本　憲(Johns Hopkins大学　放射線科)、Denis Le Bihan(Federative Institute of Research on Functional Neuroimaging、France)、伏見育崇(京都大学　画像診断学・核医学)、中島八十一(国立リハビリテーションセンター)、花川隆・福山秀直・浦山慎一(京都大学　高次脳機能センター)、平岡眞寛(京都大学　放射線科)、菊田健一郎・三國信啓・橋本信夫(京都大学　脳神経外科)、松本理器・富本秀和(京都大学　神経内科)、金柿光憲(Bordeaux大学　放射線科)、北村恵理(神戸大学　放射線科)、岡田知久(神戸中央市民病院　放射線科)、青木茂樹(東京大学　放射線科)、山田　惠(京都府立医科大学　放射線科)、滝沢　修・岡本　淳・丸山克也(シーメンス旭メディテック株式会社)

【参考文献】

1) Le Bihan D: Looking into the functional architecture of the brain with diffusion MRI. Nat Rev Neurosci 4: 469–480, 2003
2) 三木幸雄：脳疾患における拡散強調画像とMTR画像．日磁気共鳴医会誌 19：354–365，1999
3) 森　進：拡散テンソル映像法：原理と応用．認知神経科学：176–189，2005
4) Basser PJ, Pajevic S, Pierpaoli C, et al: *In vivo* fiber tractography using DT-MRI data. Magn Reson Med 44: 625–632, 2000
5) Mori S, Crain BJ, Chacko VP, et al: Three-dimensional tracking of axonal projections in the brain by magnetic resonance imaging. Ann Neurol 45: 265–269, 1999
6) Mori S, van Zijl PC: Fiber tracking: principles and strategies —a technical review. NMR Biomed 15: 468–480, 2002
7) Masutani Y, Aoki S, Abe O, et al: MR diffusion tensor imaging: recent advance and new techniques for diffusion tensor visualization. Eur J Radiol 46: 53–66, 2003
8) Lazar M, Weinstein DM, Tsuruda JS, et al: White matter tractography using diffusion tensor deflection. Hum Brain Mapp 18: 306–321, 2003
9) Sorensen AG, Wang R, Benner T, et al: An approach to validation of diffusion MRI-based white matter tractography. In: 13th Annual Meeting ISMRM. Miami Beach, 224, 2005
10) Wakana S, Jiang H, Nagae-Poetscher LM, et al: Fiber tract-based atlas of human white matter anatomy. Radiology 230: 77–87, 2004
11) Akai H, Mori H, Aoki S, et al: Diffusion tensor tractography of gliomatosis cerebri: fiber tracking through the tumor. J Comput Assist Tomogr 29: 127–129, 2005
12) Yamada K, Kizu O, Mori S, et al: Brain fiber tracking with clinically feasible diffusion-tensor MR imaging: initial experience. Radiology 227: 295–301, 2003
13) Yamada K, Kizu O, Ito H, et al: Tractography for arteriovenous malformations near the sensorimotor cortices. AJNR Am J Neuroradiol 26: 598–602, 2005
14) Clark CA, Barrick TR, Murphy MM, et al: White matter fiber tracking in patients with space-occupying lesions of the brain: a new technique for neurosurgical planning? Neuroimage 20: 1601–1608, 2003
15) Konishi J, Yamada K, Kizu O, et al: MR tractography for the evaluation of functional recovery from lenticulostriate infarcts. Neurology 64: 108–113, 2005
16) Kunimatsu A, Aoki S, Masutani Y, et al: Three-dimensional white matter tractography by diffusion tensor imaging in ischaemic stroke involving the corticospinal tract. Neuroradiology 45: 532–535, 2003
17) Abe O, Yamada H, Masutani Y, et al: Amyotrophic lateral sclerosis: diffusion tensor tractography and voxel-based analysis. NMR Biomed 17: 411–416, 2004
18) Aoki S, Iwata NK, Masutani Y, et al: Quantitative evaluation of the pyramidal tract segmented by diffusion tensor tractography: feasibility study in patients with amyotrophic lateral sclerosis. Radiat Med 23: 195–199, 2005
19) Kikuta K, Okada T, Miki Y, et al: Early experience with 3-tesla magnetic resonance tractography in the surgery of cerebral AVMs in and around the visual pathway. J Neurosurg (in press)
20) Taoka T, Sakamoto M, Iwasaki S, et al: Diffusion tensor imaging in cases with visual field defect after anterior temporal lobectomy. AJNR Am J Neuroradiol 26: 797–803, 2005
21) Powell HW, Parker GJ, Symms MR, et al: Combined fMRI and tractography reveal asymmetries in language pathways. In: 13th Annual Meeting ISMRM. Miami Beach, 764, 2005
22) Lazar M, Thottakara P, Field AS, et al: A white matter tractography study of white matter reorganization after surgical resection of brain neoplasms. In:12th Annual Meeting ISMRM. Kyoto, 1259, 2004
23) Tanenbaum LN: 3-T MR imaging: ready for clinical practice. AJNR Am J Neuroradiol 25: 1626–1627; author reply 1629, 2004
24) Nakai T, Matsuo K, Kato C, et al: BOLD contrast on a 3 T magnet: detectability of the motor areas. J Comput Assist Tomogr 25: 436–445, 2001
25) Okada T, Yamada H, Ito H, et al: Magnetic field strength increase yields significantly greater contrast-to-noise ratio increase: Measured using BOLD contrast in the primary visual area. Acad Radiol 12: 142–147, 2005
26) Fera F, Yongbi MN, van Gelderen P, et al: EPI-BOLD fMRI

of human motor cortex at 1.5 T and 3.0 T: sensitivity dependence on echo time and acquisition bandwidth. J Magn Reson Imaging **19**: 19–26, 2004

27) Graf H, Schick F, Claussen CD, et al: MR visualization of the inner ear structures: comparison of 1.5 Tesla and 3 Tesla images. Rofo **176**: 17–20, 2004

28) Hunsche S, Moseley ME, Stoeter P, et al: Diffusion-tensor MR imaging at 1.5 and 3.0 T: initial observations. Radiology **221**: 550–556, 2001

29) Fushimi Y, Miki Y, Kikuta K, et al: Three-dimensional time of flight MR angiography of Moyamoya disease: comparison of 3.0-T imaging and 1.5-T imaging: A Preliminary Study. Radiology, 2006 (in press)

30) Holodny AI, Gor DM, Watts R, et al: Diffusion-tensor MR tractography of somatotopic organization of corticospinal tracts in the internal capsule: initial anatomic results in contradistinction to prior reports. Radiology **234**: 649–653, 2005

31) Nagae-Poetscher LM, Jiang H, Wakana S, et al: High-resolution diffusion tensor imaging of the brain stem at 3 T. AJNR Am J Neuroradiol **25**: 1325–1330, 2004

32) Jaermann T, Crelier G, Pruessmann KP, et al: SENSE-DTI at 3 T. Magn Reson Med **51**: 230–236, 2004

33) 岡田　務，三木幸雄：拡散テンソル画像．susceptibility-weighted imaging．映像情報Medical **37**：976–984，2005

34) Okada T, Miki Y, Fushimi Y, et al: Diffusion tensor fiber tractography: intra-individual comparison of 3 T and 1.5 T. Radiology, 2006 (in press)

35) Legatt AD: Current practice of motor evoked potential monitoring: results of a survey. J Clin Neurophysiol **19**: 454–460, 2002

36) Keles GE, Lundin DA, Lamborn KR, et al: Intraoperative subcortical stimulation mapping for hemispherical perirolandic gliomas located within or adjacent to the descending motor pathways: evaluation of morbidity and assessment of functional outcome in 294 patients. J Neurosurg **100**: 369–375, 2004

37) Nimsky C, Ganslandt O, Hastreiter P, et al: Preoperative and intraoperative diffusion tensor imaging-based fiber tracking in glioma surgery. Neurosurgery **56**: 130–137; discussion 138, 2005

38) Coenen VA, Krings T, Axer H, et al: Intraoperative three-dimensional visualization of the pyramidal tract in a neuronavigation system (PTV) reliably predicts true position of principal motor pathways. Surg Neurol **60**: 381–390; discussion 390, 2003

39) Berman JI, Berger MS, Mukherjee P, et al: Diffusion-tensor imaging-guided tracking of fibers of the pyramidal tract combined with intraoperative cortical stimulation mapping in patients with gliomas. J Neurosurg **101**: 66–72, 2004

40) Kamada K, Todo T, Masutani Y, et al: Combined use of tractography-integrated functional neuronavigation and direct fiber stimulation. J Neurosurg **102**: 664–672, 2005

41) Okada T, Mikuni N, Miki Y, et al: Integration of diffusion tensor tractography of the corticospinal tract using 3 T with intraoperative white matter stimulation mapping: preliminary results to validate corticospinal tract localization. Radiology (in press)

42) Nimsky C, Ganslandt O, Hastreiter P, et al: Intraoperative diffusion-tensor MR imaging: shifting of white matter tracts during neurosurgical procedures—initial experience. Radiology **234**: 218–225, 2005

43) Coenen VA, Krings T, Weidemann J, et al: Sequential visualization of brain and fiber tract deformation during intracranial surgery with three-dimensional ultrasound: an approach to evaluate the effect of brain shift. Neurosurgery **56** (1 suppl): 133–141; discussion 133–141, 2005

44) Lin CP, Wedeen VJ, Chen JH, et al: Validation of diffusion spectrum magnetic resonance imaging with manganese-enhanced rat optic tracts and *ex vivo* phantoms. Neuroimage **19**: 482–495, 2003

45) Behrens TE, Woolrich MW, Jenkinson M, et al: Characterization and propagation of uncertainty in diffusion-weighted MR imaging. Magn Reson Med **50**: 1077–1088, 2003

46) Tournier JD, Calamante F, Connelly A: Improved characterisation of crossing fibres: optimisation of spherical deconvolution parameters using a minimum entropy principle. In:13th Annual Meeting ISMRM. Miami Beach, 384, 2005

47) Tuch DS: Q-ball imaging. Magn Reson Med **52**: 1358–1372, 2004

48) Jones DK: Determining and visualizing uncertainty in estimates of fiber orientation from diffusion tensor MRI. Magn Reson Med **49**: 7–12, 2003

49) Kinoshita M, Yamada K, Hashimoto N, et al: Fiber-tracking does not accurately estimate size of fiber bundle in pathological condition: initial neurosurgical experience using neuronavigation and subcortical white matter stimulation. Neuroimage **25**: 424–429, 2005

50) van Buchem MA, Udupa JK, McGowan JC, et al: Global volumetric estimation of disease burden in multiple sclerosis based on magnetization transfer imaging. AJNR Am J Neuroradiol **18**: 1287–1290, 1997

51) Miki Y, Grossman RI, Udupa JK, et al: Differences between relapsing-remitting and chronic progressive multiple sclerosis as determined with quantitative MR imaging. Radiology **210**: 769–774, 1999

52) Phillips MD, Grossman RI, Miki Y, et al: Comparison of T2 lesion volume and magnetization transfer ratio histogram analysis and of atrophy and measures of lesion burden in patients with multiple sclerosis. AJNR Am J Neuroradiol

19: 1055–1060, 1998
53) 三木幸雄：多発性硬化症の脳病態と画像．臨床放射線 44：1317–1322，1999
54) van der Flier WM, van den Heuvel DM, Weverling-Rijnsburger AW, et al: Magnetization transfer imaging in normal aging, mild cognitive impairment, and Alzheimer's disease. Ann Neurol 52: 62–67, 2002
55) Rovaris M, Iannucci G, Cercignani M, et al: Age-related changes in conventional, magnetization transfer, and diffusion-tensor MR imaging findings: study with whole-brain tissue histogram analysis. Radiology 227: 731–738, 2003
56) Yamamoto A, Miki Y, Adachi S, et al: Whole brain magnetization transfer histogram analysis of pediatric acute lymphoblastic leukemia patients receiving intrathecal methotrexate therapy. Eur J Radiol (in press)
57) Inglese M, Salvi F, Iannucci G, et al: Magnetization transfer and diffusion tensor MR imaging of acute disseminated encephalomyelitis. AJNR Am J Neuroradiol 23: 267–272, 2002
58) Yoshiura T, Mihara F, Tanaka A, et al: Age-related structural changes in the young adult brain shown by magnetic resonance diffusion tensor imaging. Acad Radiol 12: 268–275, 2005
59) Ragin AB, Storey P, Cohen BA, et al: Whole brain diffusion tensor imaging in HIV-associated cognitive impairment. AJNR Am J Neuroradiol 25: 195–200, 2004
60) Arzoumanian Y, Mirmiran M, Barnes PD, et al: Diffusion tensor brain imaging findings at term-equivalent age may predict neurologic abnormalities in low birth weight preterm infants. AJNR Am J Neuroradiol 24: 1646–1653, 2003
61) Sach M, Winkler G, Glauche V, et al: Diffusion tensor MRI of early upper motor neuron involvement in amyotrophic lateral sclerosis. Brain 127: 340–350, 2004
62) 福山秀直：SPMを用いたPET，SPECTによる脳賦活試験法．http://www.cybernet.co.jp/matlab/industries/biotech/stories.shtml
63) Ashburner J, Friston KJ: Voxel-based morphometry－the methods. Neuroimage 11: 805–821, 2000
64) Good CD, Johnsrude IS, Ashburner J, et al: A voxel-based morphometric study of ageing in 465 normal adult human brains. Neuroimage 14: 21–36, 2001
65) Gaser C, Nenadic I, Buchsbaum BR, et al: Deformation-based morphometry and its relation to conventional volumetry of brain lateral ventricles in MRI. Neuroimage 13: 1140–1145, 2001
66) Leung LH, Ooi GC, Kwong DL, et al: White-matter diffusion anisotropy after chemo-irradiation: a statistical parametric mapping study and histogram analysis. Neuroimage 21: 261–268, 2004
67) Burns J, Job D, Bastin ME, et al: Structural disconnectivity in schizophrenia: a diffusion tensor magnetic resonance imaging study. Br J Psychiatry 182: 439–443, 2003
68) Eriksson SH, Rugg-Gunn FJ, Symms MR, et al: Diffusion tensor imaging in patients with epilepsy and malformations of cortical development. Brain 124: 617–626, 2001
69) Thivard L, Lehericy S, Krainik A, et al: Diffusion tensor imaging in medial temporal lobe epilepsy with hippocampal sclerosis. Neuroimage 28: 682–690, 2005
70) Jones DK, Symms MR, Cercignani M, et al: The effect of filter size on VBM analyses of DT-MRI data. Neuroimage 26: 546–554, 2005

Diffusion-Tensor Fiber Tractography: Intraindividual Comparison of 3.0-T and 1.5-T MR Imaging[1]

Tsutomu Okada, MD
Yukio Miki, MD, PhD
Yasutaka Fushimi, MD
Takashi Hanakawa, MD, PhD
Mitsunori Kanagaki, MD, PhD
Akira Yamamoto, MD
Shin-ichi Urayama, PhD
Hidenao Fukuyama, MD, PhD
Masahiro Hiraoka, MD, PhD
Kaori Togashi, MD, PhD

Purpose: To prospectively evaluate the depiction of brain fiber tracts at 3.0- versus 1.5-T diffusion-tensor (DT) fiber tractography performed with parallel imaging.

Materials and Methods: Institutional review board approval was obtained, and each subject provided written informed consent. Subjects were 30 healthy volunteers (15 men, 15 women; mean age, 28 years; age range, 21–46 years). Single-shot spin-echo echo-planar magnetic resonance (MR) sequences with parallel imaging were applied. Four fiber tracts were reconstructed: corticospinal tract (CST), superior longitudinal fasciculus (SLF), corpus callosum (CC), and fornix. Two neuroradiologists compared 3.0- and 1.5-T tractography in terms of fiber tract depiction by using five depiction scores (scores 0–4) and numbers of reconstructed tract fibers and in terms of lateral asymmetry in the CST by using numbers of reconstructed fibers. The Wilcoxon signed rank test was applied for statistical analysis.

Results: Visual scores for both CST hemispheres ($P < .001$), the right SLF ($P = .005$), the CC ($P = .01$), and the right fornix ($P = .04$) were higher at 3.0-T DT tractography. Larger numbers of CST (right, $P = .008$; left, $P < .001$), SLF (right, $P = .001$; left, $P = .02$), and fornix (bilaterally, $P = .02$) tract fibers were depicted at 3.0 T. The asymmetry index for the CST was lower ($P < .001$) at 3.0 T. Visual scores for the left SLF and the left fornix and numbers of CC tract fibers were not significantly different.

Conclusion: Depiction of most fiber tracts was improved at 3.0-T DT tractography compared with depiction at 1.5-T tractography.

[1] From the Department of Diagnostic Imaging and Nuclear Medicine (T.O., Y.M., Y.F., M.K., A.Y., K.T.) and Department of Therapeutic Radiology and Oncology (M.H.), Graduate School of Medicine, and Human Brain Research Center (T.H., S.U., H.F.), Kyoto University, 54 Kawahara-cho, Shogoin, Sakyo-ku, Kyoto-shi, Kyoto 606-8507, Japan. From the 2004 RSNA Annual Meeting. Received December 30, 2004; revision requested March 17, 2005; revision received May 4; final version accepted June 1. Supported in part by grants from the Ministry of Health, Labor and Welfare of Japan (k0800006-01) and the Ministry of Education Culture, Sports, Science and Technology of Japan (C)(15591270).

Diffusion-tensor (DT) imaging is a magnetic resonance (MR) imaging technique that is sensitive to the orientation of mobility in intravoxel water molecules (1,2). DT imaging reveals two specific characteristics: diffusion anisotropy and the directional distribution of water diffusivity. When water diffusion in a tissue is almost the same in all directions, the diffusion is considered to be isotropic and have lower anisotropy. Conversely, when water diffusion is restricted along a specific direction, the diffusion is considered to be anisotropic and have higher anisotropy. Brain white matter has high diffusion anisotropy because diffusion is faster when it is parallel to the fiber direction than when it is the same in all other directions (3,4).

DT images of the human brain can be reconstructed for visualization of the macroscopic three-dimensional fiber tract architecture by using a process known as fiber tractography, or the fiber-tracking technique (5–10). DT imaging and fiber tractography are powerful tools for studying cerebral white matter and have been applied clinically to assess brain tumors (11,12), diffuse axonal injury (13), pediatric brain development (14), and cerebral infarcts (15).

With recent advances in actively shielded 3.0-T magnets, the use of high-field-strength MR imaging in clinical settings has become practical (16,17). Parallel imaging techniques, such as simultaneous acquisition of spatial harmonics, or SMASH (18); sensitivity encoding (19); and auto-SMASH–based generalized autocalibrating partially parallel acquisition (20), also have improved with recent advances in MR imaging hardware. Owing to shortened echo train lengths and echo times, parallel imaging techniques can be used to reduce artifacts related to spin-echo echo-planar imaging. Some reports have described the performance of parallel imaging in spin-echo echo-planar DT imaging and fiber tractography at 1.5 or 3.0 T (9,10,21–24). However, to our knowledge, in no reports have the differences between 3.0- and 1.5-T spin-echo echo-planar DT fiber tractography with parallel imaging been compared. Thus, the purpose of our study was to prospectively evaluate the depiction of brain fiber tracts at 3.0-T versus 1.5-T DT fiber tractography performed with parallel imaging.

Materials and Methods

Study Subjects

The study population comprised 30 healthy volunteers (15 men, 15 women; mean age, 28 years; age range, 21–46 years) with no history of neurologic injury or psychiatric disease. All subjects were examined by one of the authors (T.H., with 14 years of experience as a neurologist), and no subjects had abnormal neurologic signs or symptoms. Institutional review board approval was obtained for this study, and each subject provided written informed consent.

Data Acquisition

All subjects underwent 3.0- and 1.5-T DT imaging, which was performed by using a whole-body 3.0-T MR unit (Trio; Siemens, Erlangen, Germany) with a 40 mT/m gradient and a 1.5-T MR unit (Symphony; Siemens) with a 30 mT/m gradient, on the same day. MR imaging at 3.0 T was performed by one author (T.O.), and MR imaging at 1.5 T was performed by another author (Y.F.), both of whom had 8 years of experience as neuroradiologists and 2 years of experience in DT imaging. The time delay between 3.0- and 1.5-T MR imaging was less than 1 hour for all subjects. Both MR units were equipped with integrated parallel acquisition capability and a receive-only eight-channel phased-array head coil. Both the 3.0-T and the 1.5-T DT imaging examinations involved the use of single-shot spin-echo echo-planar sequences and nearly identical parameters: 5200/79 (repetition time msec/echo time msec), a 220-mm field of view, a 128 × 128 matrix, 3-mm section thickness without intersection gaps (matrix size, 1.7 × 1.7 × 3.0 mm), and four repetitions.

The generalized autocalibrating partially parallel acquisition algorithm was applied for parallel imaging with use of a reduction factor of two, 24 additional autocalibrating phase-encoding steps in the center of k-space, and a 75% partial Fourier technique in the phase-encoding direction. Only the bandwidths differed: A bandwidth of 1502 Hz per pixel was used for 3.0-T imaging, and a bandwidth of 1056 Hz per pixel was used for 1.5-T imaging. Motion-probing gradients were applied along 12 noncolinear directions with a b factor of 700 sec/mm^2 after one non–diffusion-weighted image (b = 0 sec/mm^2) was obtained. A total of 40 sections encompassed the entire cerebral hemisphere and the brainstem. The imaging times for 3.0- and 1.5-T DT imaging were almost the same—about 7.5 minutes.

Data Processing

DT imaging data sets were transferred, in Digital Imaging and Communications in Medicine format, to a Windows personal computer (IBM, New York, NY) workstation. DtiStudio, version 1.02, software (H. Jiang, S. Mori, Department of Radiology, Johns Hopkins University, Baltimore, Md) was used for tensor calculations (6,10). All source images from the DT imaging data sets were visually inspected by one author (T.O.), and images with visually apparent artifacts due to bulk motion were removed. In our DT imaging data set, there was low eddy current–related

Published online before print
10.1148/radiol.2382042192

Radiology 2006; 238:668–678

Abbreviations:
DT = diffusion tensor
ROI = region of interest

Author contributions:
Guarantors of integrity of entire study, T.O., Y.M., K.T.; study concepts/study design or data acquisition or data analysis/interpretation, all authors; manuscript drafting or manuscript revision for important intellectual content, all authors; approval of final version of submitted manuscript, all authors; literature research, T.O., Y.M., Y.F., H.F., M.H., K.T.; clinical studies, T.O., Y.M., Y.F., T.H., M.K., A.Y., S.U., K.T.; statistical analysis, T.O., Y.M., M.K., A.Y., M.H., K.T.; and manuscript editing, all authors

Address correspondence to Y.M.
(e-mail: *mikiy@kuhp.kyoto-u.ac.jp*).

Authors stated no financial relationship to disclose.

geometric distortion between images obtained in each motion-probing gradient direction (23,25), so postprocessing distortion correction was not applied for this data set. After calculating the six independent elements of the 3 × 3 tensor and diagonalization, three eigenvalues and three eigenvectors were obtained (1,3–5). The eigenvector associated with the largest eigenvalue was assumed to represent the intravoxel fiber orientation. The fractional anisotropy map and directional color-coded map were synthesized (Fig 1). Fiber orientations were assigned specific colors on the color-coded map, as follows: Red represented the right-to-left orientation; green, the anterior-to-posterior orientation; and blue, the superior-to-inferior orientation (26).

Fiber Tractography

The DtiStudio software was used to also perform fiber tractography on the basis of the fiber assignments derived by means of the continuous tracking method (6,9,10). With this software, tracking from all the pixels inside the brain (ie, with the brute force approach) was performed, and tracking results that penetrated the two manually segmented regions of interest (ROIs) on the basis of the known anatomic distributions of tracts were assigned to specific tracts (ie, with the two-ROI approach). Propagation in each fiber tract was terminated if a voxel with a fractional anisotropy value of less than 0.2 was reached or if the inner product of two consecutive vectors was greater than 0.75. These conditions prohibited the turning of angles larger than 41° during tracking (10).

Four fiber bundles—the corticospinal tract, the superior longitudinal fasciculus, the corticocortical connection fibers through the corpus callosum, and the limbic fibers through the fornix—were reconstructed by drawing specific ROIs according to the anatomic distributions of each fiber tract. ROI manipulations were performed by one neuroradiologist (A.Y.) with 3 years of experience performing tractography and 10 years of experience as a neuroradiologist. This author was blinded as to whether the images had been obtained by using 3.0 T or 1.5 T when he performed each ROI segmentation.

For corticospinal tract tractography, two ROIs were placed on transverse non–diffusion-weighted (b = 0 sec/mm^2) images (10,12,15) according to established anatomic landmarks: The first ROI was placed in the cerebral peduncle bilaterally, and the second ROI was placed in the precentral gyrus bilaterally (27) (Fig 2a).

The superior longitudinal fasciculus was reconstructed at tractography by placing two ROIs in the cerebral deep white matter on a coronal directional color-coded map. The superior longitudinal fasciculus was identified on the coronal color-coded map as a region where the fiber orientation was anterior to posterior (green), lateral to the corona radiata (26,28). An anterior ROI was placed in the plane passing through the reconstructed corticospinal tract, and a posterior ROI was placed in the plane passing through the rostral surface of the splenium of the corpus callosum, with both ROIs covering the green area representing the superior longitudinal fasciculus (Fig 2c). Some "noise" fibers that were apparently tracing the error course were then removed (10).

Corpus callosum tractography was performed by imaging the combination of four different callosal fiber bundles. The primary ROI was placed in the corpus callosum in the midsagittal plane (Fig 2d). To visualize different parts of the callosal fibers, secondary ROIs were placed in four regions: two ROIs on the coronal color-coded map and two ROIs on the transverse color-coded map (Fig 2e). Anterior callosal fibers, referred to as minor forceps, were reconstructed by placing the ROI covering the deep white matter in the coronal plane anterior to the genu of the corpus callosum. For reconstruction of the posterior cal-

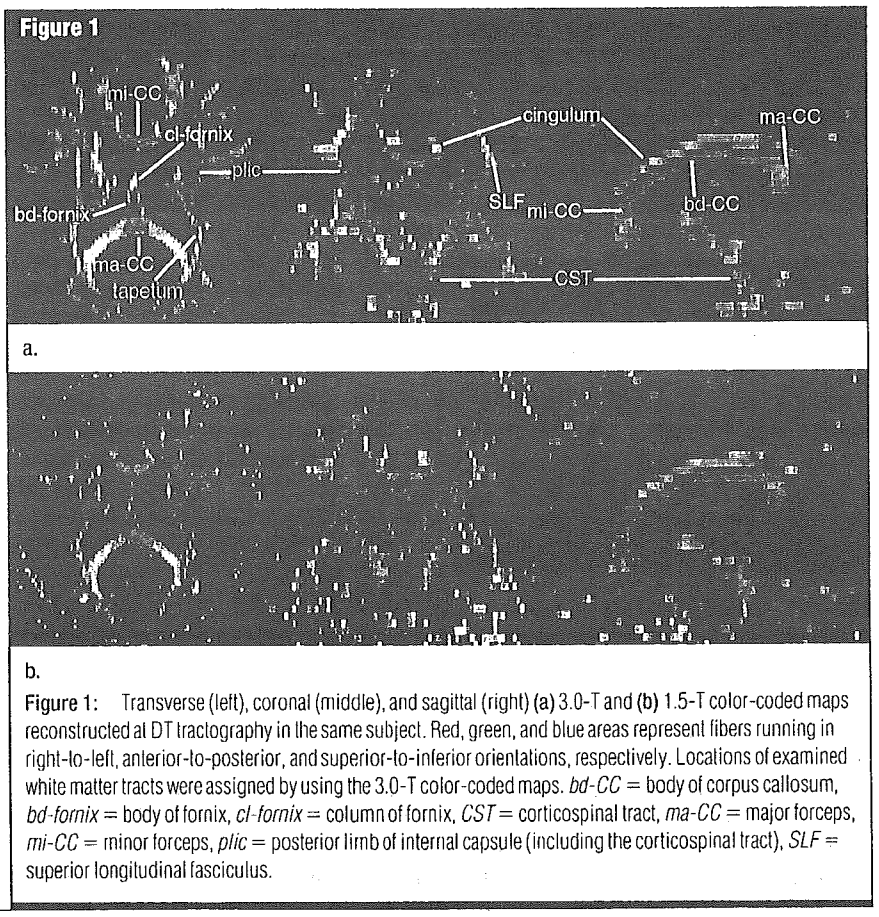

Figure 1: Transverse (left), coronal (middle), and sagittal (right) **(a)** 3.0-T and **(b)** 1.5-T color-coded maps reconstructed at DT tractography in the same subject. Red, green, and blue areas represent fibers running in right-to-left, anterior-to-posterior, and superior-to-inferior orientations, respectively. Locations of examined white matter tracts were assigned by using the 3.0-T color-coded maps. *bd-CC* = body of corpus callosum, *bd-fornix* = body of fornix, *cl-fornix* = column of fornix, *CST* = corticospinal tract, *ma-CC* = major forceps, *mi-CC* = minor forceps, *plic* = posterior limb of internal capsule (including the corticospinal tract), *SLF* = superior longitudinal fasciculus.

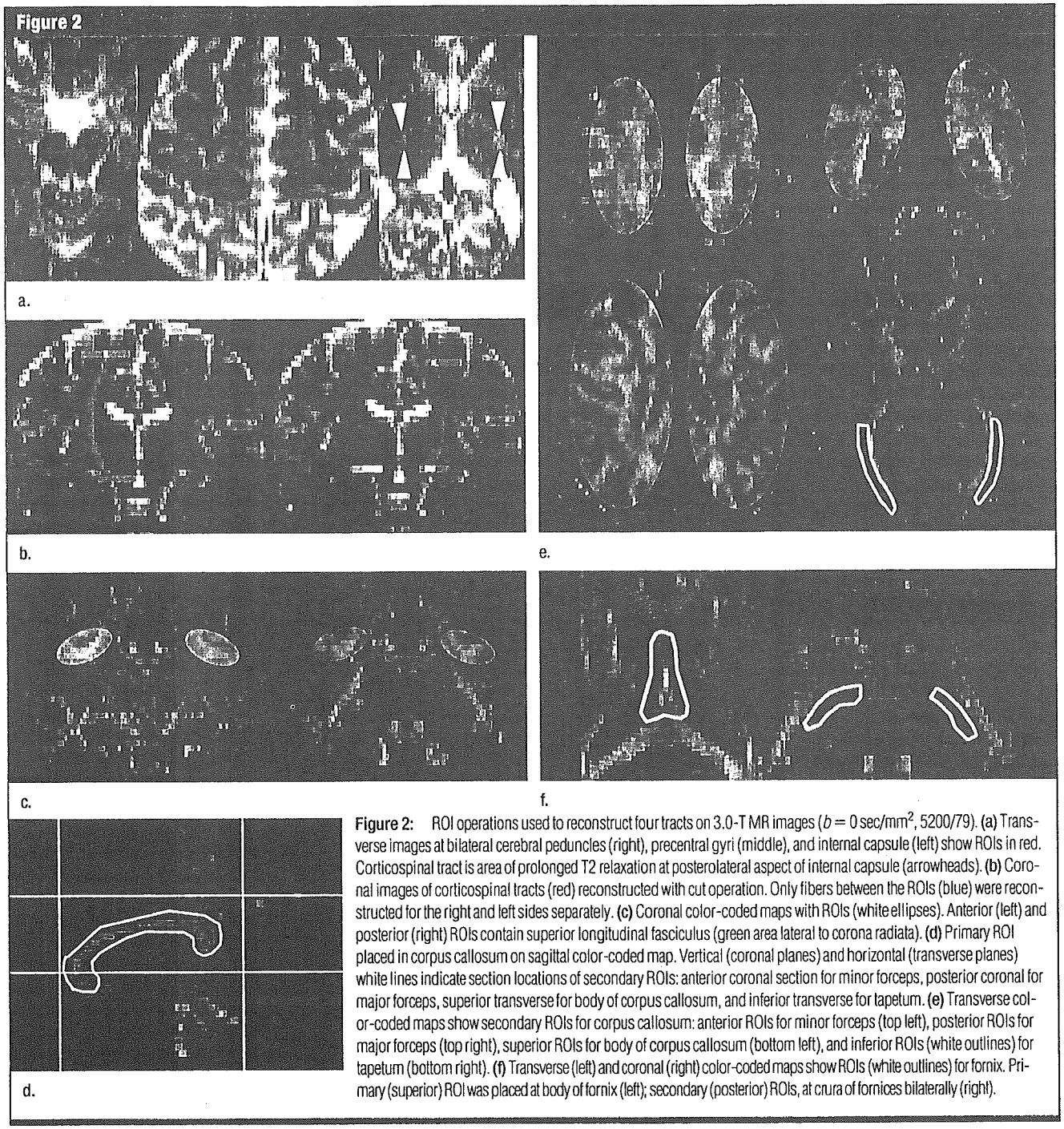

Figure 2: ROI operations used to reconstruct four tracts on 3.0-T MR images ($b = 0$ sec/mm^2, 5200/79). **(a)** Transverse images at bilateral cerebral peduncles (right), precentral gyri (middle), and internal capsule (left) show ROIs in red. Corticospinal tract is area of prolonged T2 relaxation at posterolateral aspect of internal capsule (arrowheads). **(b)** Coronal images of corticospinal tracts (red) reconstructed with cut operation. Only fibers between the ROIs (blue) were reconstructed for the right and left sides separately. **(c)** Coronal color-coded maps with ROIs (white ellipses). Anterior (left) and posterior (right) ROIs contain superior longitudinal fasciculus (green area lateral to corona radiata). **(d)** Primary ROI placed in corpus callosum on sagittal color-coded map. Vertical (coronal planes) and horizontal (transverse planes) white lines indicate section locations of secondary ROIs: anterior coronal section for minor forceps, posterior coronal for major forceps, superior transverse for body of corpus callosum, and inferior transverse for tapetum. **(e)** Transverse color-coded maps show secondary ROIs for corpus callosum: anterior ROIs for minor forceps (top left), posterior ROIs for major forceps (top right), superior ROIs for body of corpus callosum (bottom left), and inferior ROIs (white outlines) for tapetum (bottom right). **(f)** Transverse (left) and coronal (right) color-coded maps show ROIs (white outlines) for fornix. Primary (superior) ROI was placed at body of fornix (left); secondary (posterior) ROIs, at crura of fornices bilaterally (right).

losal fibers, referred to as major forceps, the ROI was placed posterior to the splenium of the corpus callosum. Callosal body fibers were reconstructed by placing the ROI at the centrum semiovale in the transverse plane superior to the body of the corpus callosum. For reconstruction of the temporal interhemispheric connection fibers, referred to as tapetum, ROIs were placed bilaterally in the temporal deep white matter, lateral to the trigon of the lateral ventricles. These four fibers (ie, minor forceps, major forceps, callosal body fibers, and tapetum) were combined to delineate the entire corpus callosum.

Limbic fibers through the fornix were reconstructed by placing one primary ROI and two secondary ROIs. The primary ROI was placed in the body of the fornix, and the secondary ROIs

Figure 3

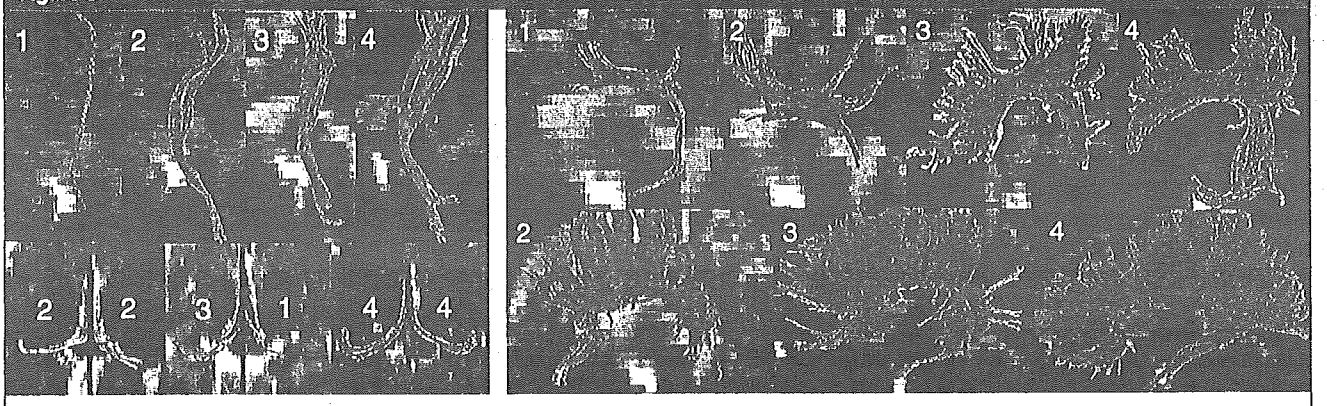

a. b.

Figure 3: Scoring (scores *1–4*) for fiber tract depiction at tractography. Red areas represent the depicted tracts. **(a)** Top: Corticospinal tractographic image superimposed on sagittal non–diffusion-weighted images (5200/79) viewed from left side. Grades *1* and *2* were assigned at 1.5-T imaging, and grades *3* and *4* were assigned at 3.0-T imaging. Bottom: Fornix tractographic image obtained at 3.0 T superimposed on transverse non–diffusion-weighted images (5200/79). Blue lines separate right and left fornix tractographic images. **(b)** Superior longitudinal fasciculus tractographic image (top) and corpus callosum tractographic image (bottom) superimposed on sagittal non–diffusion-weighted images (5200/79) viewed from left side. For superior longitudinal fasciculus tractography (top), grades 1 and 2 were assigned at 1.5-T imaging, and grades 3 and 4 were assigned at 3.0-T imaging. For corpus callosum tractography, grade 2 was assigned at 1.5 T imaging, and grades 3 and 4 were assigned at 3.0-T imaging. In no subject was grade 1 assigned at corpus callosum tractography.

were placed in the crura of the right and left fornices anterolateral to the splenium of the corpus callosum (Fig 2f).

Evaluation of Tractography

The tractographic depiction of fiber tracts was graded on three-dimensional volume views and in three orthogonal two-dimensional planes by two neuroradiologists (T.O., with 2 years of experience performing tractography; Y.M., with 3 years of experience performing tractography and 19 years of experience as a neuroradiologist). Grading was performed on the basis of the following three criteria: the fiber tract volume, the anatomic distribution of the tract, and the presence or absence of the tract at the expected location. The readers were blinded to the magnetic field strength used (1.5 or 3.0 T). After performing independent interpretations, the two readers resolved any score discrepancies by consensus to establish final scores.

One score was derived from one tractographic examination—not from the pair of ROIs used to perform reconstructing tractography. The scores assigned at fiber tractography were as follows: 4 meant excellent—that is, the depicted fiber tract accurately matched the known anatomic distribution, and there was a sufficient volume of fibers; 3 meant adequate for diagnosis—that is, imaging errors such as image distortion and tract propagation error were minor, so the image was still adequate for use as a diagnostic tool; 2 meant fair—that is, moderate imaging errors or moderate tract volume loss markedly reduced imaging quality; 1 meant poor—that is, there were major imaging errors and/or tract volume loss, and the readers were unable to interpret the course or shape of the tract; and 0 meant no tract visualization.

At corticospinal tract tractography, anatomically accurately depicted tracts were defined as those passing through the lateral segment of the cerebral peduncle, the posterior limb of the internal capsule, and the precentral gyrus. At superior longitudinal fasciculus tractography, fibers connecting the frontal and parietal lobes (ie, long association fibers) and fibers connecting the frontal and temporal lobes (ie, arcuate fibers) were considered. Anatomically accurate results for the superior longitudinal fasciculus were defined as good visualization of both the long association fibers and the arcuate fibers. At corpus callosum tractography, anatomically accurate results were defined as good visualization of the four different subsegments. At limbic tractography, the depiction of fibers connecting the column, body, and crus of the fornix was considered to represent anatomically accurate results. At tractography, the depicted superior longitudinal fasciculus, corpus callosum, and fornix are each composed of several subsegments of fiber bundles, and all subsegments were integrated to establish a single final score for each tractographic examination. The scoring of tractographic images is illustrated in Figure 3.

Tractographic depictions of the corticospinal tract, superior longitudinal fasciculus, and fornix on the right and left sides were assessed independently. At corpus callosum tractography, the right and left sides were assessed together, because callosal fiber connects the right and left hemispheres.

Reconstructed tract fibers were counted by using the DtiStudio software. The numbers of fibers depicted at tractography of the corticospinal tract and the superior longitudinal fasciculus in the right and left hemispheres were counted separately. The right and left fibers were not counted separately at tractography of the corpus callosum and

the fornix, because right- and left-hemisphere limbic fibers were difficult to differentiate at the column of the fornix, which was visualized as a single fiber bundle.

Although the diffusion characteristics of the normal brain are somewhat asymmetric, corticospinal tract tractography in healthy subjects reportedly reveals minimal asymmetry (17,29). To assess the reliability of corticospinal tract tractography in healthy subjects, lateral asymmetry was evaluated on the basis of the numbers of right- and left-hemisphere fibers at tractography of the corticospinal tract. For this purpose, the "cut" operation was performed by using DtiStudio software. With the cut operation, only the fiber coordinates between the two ROIs are reconstructed (Fig 2b). The conventional two-ROI approach involves the use of three corticospinal tract regions at tractography: the areas below the cerebral peduncle, between the two ROIs, and above the precentral gyrus. These three regions have very different properties. In the region between the two ROIs, tracking results do not branch and are more robust against noise. This approach is particularly useful for quantitative analysis.

The index of asymmetry (AI) between the right *(R)* and left *(L)* corticospinal tracts in each subject at tractography was calculated as the absolute difference in fiber numbers between the two sides, divided by the mean of the two sides, as modified from a previously described method (14): $AI = L - R / \{(L + R)/2\}$. Lateral asymmetry analysis of superior longitudinal fasciculus tractography was not performed, because the superior longitudinal fasciculus comprises numerous long and short connecting fibers and lateral asymmetry is commonly observed in healthy subjects (6,29).

Statistical Analyses

Differences between 3.0- and 1.5-T DT imaging were calculated in terms of the following features: *(a)* depiction scores for right and left corticospinal tract tractography, right and left superior longitudinal fasciculus tractography, corpus callosum tractography, and right and left fornix tractography; *(b)* numbers of fibers depicted at right and left tractography of the corticospinal tract, right and left tractography of the superior longitudinal fasciculus, corpus callosum tractography, and fornix tractography; and *(c)* asymmetry index at corticospinal tract tractography. Statistical

Figure 4

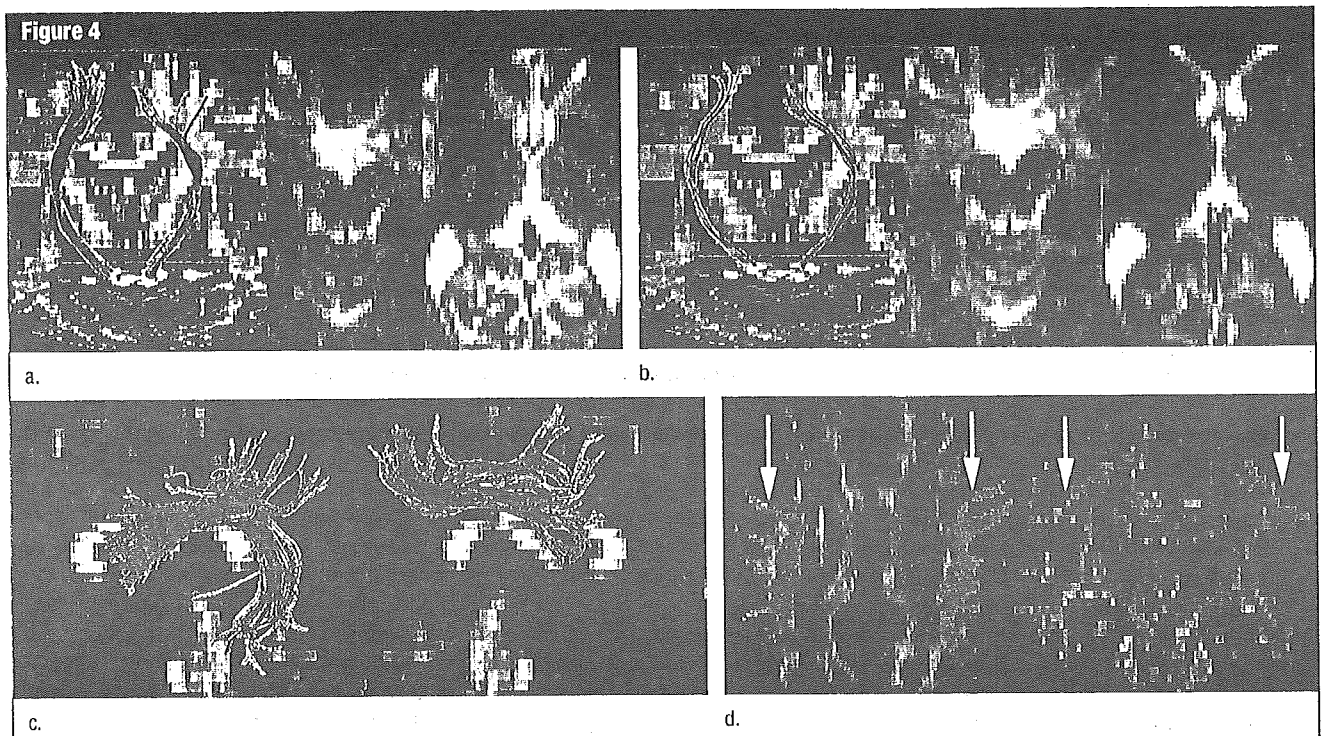

Figure 4: Fiber tractographic results. **(a, b)** Left: Three-dimensional reconstruction of corticospinal tract (red) in the same subject at **(a)** 3.0-T and **(b)** 1.5-T tractography, with use of transverse and coronal fractional anisotropy images. Middle and right: Transverse non–diffusion-weighted images with two-dimensional overlays of tractographic images at the sections of the cerebral peduncles (middle) and internal capsule (right) bilaterally. The voxels where the depicted corticospinal tract penetrates the transverse planes are shaded red. At 1.5-T corticospinal tract tractography (b), although the proper anatomic distribution is depicted, the tract volume is lower than that at 3.0 T. **(c)** Three-dimensional reconstruction of superior longitudinal fasciculus (red) on sagittal fractional anisotropy map at 3.0-T tractography in a different subject. At tractography in this subject, the shapes and distributions of the right and left superior longitudinal fasciculi differed. Although tractography of the left superior longitudinal fasciculus depicted arcuate fibers toward the temporal lobe, tractography of the right superior longitudinal fasciculus depicted no arcuate fibers. The corticocortical long connection fibers between the frontal and parietal lobes, however, were thicker on the right side than on the left side. **(d)** Tractographic image of superior longitudinal fasciculus (red, arrows) overlaid on 3.0-T transverse (left) and coronal (right) color-coded maps obtained in the subject described in c *(Fig 4 continues).*

analysis was based on the consensus scores for each tract in each subject derived by the two neuroradiologists. The Wilcoxon signed rank test was applied by using JMP, version 5.1, software (SAS Institute, Cary, NC). For all statistical analyses, $P < .05$ was considered to be indicative of a significant difference.

Results

Fiber Tract Visualization

DT imaging at both 3.0 and 1.5 T was successfully performed in all 30 subjects. The corticospinal tract was visualized at 3.0 and 1.5 T (Fig 4a, 4b) in all subjects. At superior longitudinal fasciculus tractography, long association fibers were visualized in all subjects at 3.0 and 1.5 T. Right arcuate fibers were visualized in 22 subjects (73%) at 3.0 T and in 20 subjects (67%) at 1.5 T, whereas left arcuate fibers were identified in 29 subjects (97%) at 3.0 and 1.5 T (Fig 4c, 4d).

All four subsegments of the corpus callosum were successfully visualized at 3.0 and 1.5 T (Fig 4e) in every subject. The body and column of the fornix were visualized at 3.0 and 1.5 T in every subject. The right crus of the fornix was visualized in 21 subjects (70%) at 3.0 T and in 18 subjects (60%) at 1.5 T. The left crus of the fornix was visualized in 27 subjects (90%) at 3.0 T and in 25 subjects (83%) at 1.5 T (Fig 4f). One subject was incidentally found to have cavum septum pellucidum and cavum vergae. The right and left columns of the fornix were visualized separately in this subject (Fig 4g).

All tractographic results were included in the analysis of tract depiction scores and numbers of depicted tract fibers. All tractographic results for the corticospinal tract were included for asymmetry analysis. With regard to the 420 depiction scores (30 subjects times seven tracts times two readers), there were discrepancies between the two independent readers regarding 152 scores (36%). The two readers discussed the discrepancy and established a final consensus score in each case. The depicted fiber tracts and the depiction scores are listed in Table 1.

Statistical Analyses

For tractography of the corticospinal tract, both right- and left-hemisphere depiction scores ($P < .001$) and numbers of tract fibers (right, $P = .008$; left, $P < .001$) were significantly higher at 3.0 T than at 1.5 T. The asymmetry index at corticospinal tract tractography was significantly lower at 3 T ($P < .001$). For tractography of the right su-

Figure 4

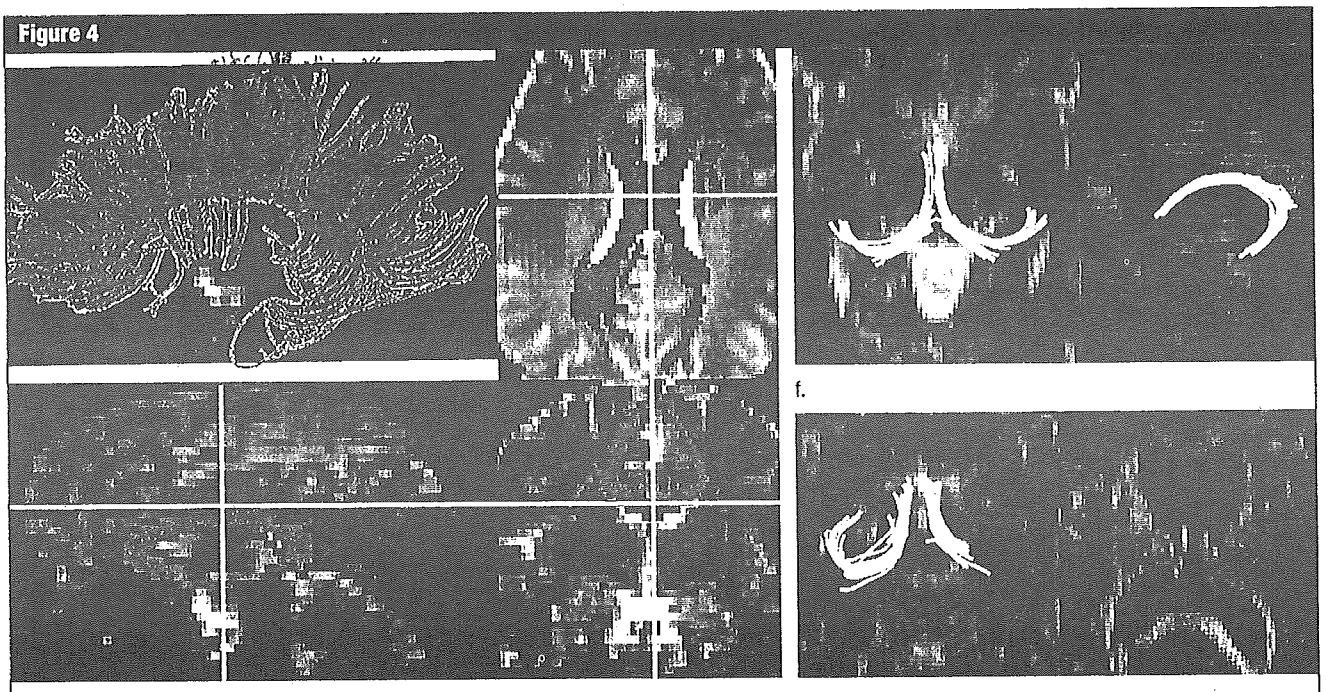

Figure 4 *(continued)*: **(e)** Three-dimensional 3.0-T tractographic reconstruction of corpus callosum (red) on sagittal non–diffusion-weighted image (5200/79) (top left) and on overlay in three orthogonal planes (top right, bottom left, and bottom right). Various kinds of transcallosal connection fibers are depicted. The center indicated by the intersecting of the vertical and horizontal lines on the three orthogonal images (top right, bottom left, and bottom right) indicate the same location. **(f)** Three-dimensional 3.0-T tractographic reconstruction of fornix (yellow) on transverse non–diffusion-weighted image (5200/79) (left) and sagittal color-coded map viewed from left (right). **(g)** Three-dimensional 3.0-T tractographic reconstruction of fornix (yellow) on transverse non–diffusion-weighted image (5200/79) (left) and transverse color-coded map (right) obtained in a subject with cavum septum pellucidum and cavum vergae. The bodies and columns of the fornices on the right and left sides were visualized separately.

perior longitudinal fasciculus, depiction scores ($P = .005$) and numbers of tract fibers ($P = .001$) were significantly higher at 3.0 T than at 1.5 T. Depiction scores for tractography of the left superior longitudinal fasciculus did not differ significantly between 3.0- and 1.5-T DT imaging. For tractography of the left superior longitudinal fasciculus, the numbers of tract fibers were significantly higher at 3.0 T than at 1.5 T ($P = .02$). For corpus callosum tractography, depiction scores were significantly higher at 3.0 T than at 1.5 T ($P = .01$), although the numbers of tract fibers did not differ significantly. Scores for depiction of the right fornix ($P = .04$) and numbers of fornix tract fibers bilaterally ($P = .02$) were significantly higher at 3.0 T than at 1.5 T, although scores for depiction of the left fornix were not significantly different. These results are summarized in Table 2.

Table 1

Depiction Scores Assigned at Fiber Tractography

Tract and Score	3.0-T Tractography	1.5-T Tractography
Right corticospinal tract		
0	0	0
1	0	2
2	1	8
3	6	13
4	23	7
Left corticospinal tract		
0	0	0
1	0	6
2	1	9
3	6	10
4	23	5
Right superior longitudinal fasciculus		
0	0	0
1	1	3
2	10	11
3	6	9
4	13	7
Left superior longitudinal fasciculus		
0	0	0
1	1	0
2	3	3
3	14	17
4	12	10
Corpus callosum		
0	0	0
1	0	0
2	2	6
3	9	14
4	19	10
Right fornix		
0	0	0
1	10	11
2	8	16
3	11	3
4	1	0
Left fornix		
0	0	0
1	3	4
2	14	17
3	12	9
4	1	0

Note.—Data are numbers of subjects with the given depiction score. Scores were determined in consensus between two readers.

Discussion

In recent studies, investigators have reported on intraindividual comparisons between 3.0- and 1.5-T DT imaging performed for functional MR imaging based on blood oxygen level–dependent contrast (30), intracranial time-of-flight MR angiography (31), supraaortic contrast material–enhanced MR angiography (32), and high-spatial-resolution inner ear imaging (33). These studies revealed the clinical feasibility of and the better visualization that is achievable at 3.0-T imaging compared with these features at 1.5-T imaging. DT imaging also reportedly yields a higher signal-to-noise ratio at 3.0 T, suggesting the possibility that it renders higher spatial resolution without enhanced noise-related errors (22,34).

Parallel imaging techniques involve the use of multiple receiver coil elements for spatial information encoding and gradient encoding and, owing to shortened echo train lengths, have been shown to markedly reduce the number of echo-planar imaging–related artifacts. The potential of parallel imaging for DT imaging has been demonstrated at both 1.5 and 3.0 T (21,22). Naganawa et al (23) challenged the optimization of 3.0-T DT fiber tractography performed with parallel imaging and found that DT imaging data on brain fiber tracking in healthy subjects can be acquired within a very short imaging time (<2 minutes). Nagae-Poetscher et al (24) performed high-spatial-resolution DT imaging of the brainstem at 3.0 T with parallel imaging and visualized various brainstem structures, including deep cerebellar nuclei, some cranial nerves, and white matter tracts.

To our knowledge, our study is the first in which the findings of 3.0- and

1.5-T DT fiber tractography, both performed with parallel imaging, were compared in a relatively large number of subjects. Improved image quality was observed at 3.0-T tractography of the corticospinal tract.

More complex results were observed at tractography of the superior longitudinal fasciculus. Although the right superior longitudinal fasciculus was visualized significantly better at 3.0 T, the depiction score for left superior longitudinal fasciculus tractography did not differ significantly between 3.0 and 1.5 T. The numbers of tract fibers depicted at 3.0 T were significantly higher than the numbers of fibers depicted at 1.0 T. We speculated that the reason for this was as follows: According to fiber dissection study findings, the corticospinal tract is a long projection fiber bundle with a well-established anatomic distribution (35). Most fibers in the corticospinal tract run parallel through the posterior limb of the internal capsule, without sharp turning angles or directional diversity.

Conversely, both the superior longitudinal fasciculus and the corpus callosum consist of groups of fiber bundles that comprise association or commissural fibers of varying lengths and directions. The superior longitudinal fasciculus contains arcuate fibers that turn sharply toward the temporal lobe. This sharp turning angle may surpass the tracking terminate threshold, and tracking does not extend to reach the temporal lobe. Temporal fibers are susceptible to image distortion at the middle cranial fossa and temporal bone, where the air-tissue interface induces magnet susceptibility artifacts. Thus, we propose that temporal arcuate fibers are more affected by image distortion than are long association fibers. In the present study, left arcuate fibers were visualized in a larger number of subjects than were right arcuate fibers at both 3.0 and 1.5 T. Such asymmetry of the arcuate fibers at tractography may be due to image distortion or the known lateral asymmetry of temporal fibers (36), and, thus, differences between 3.0- and 1.5-T DT imaging may be underestimated on the left side.

Table 2

Analyses of Tract Depiction Scores and Numbers of Tract Fibers

Tract	Difference in Depiction Score*	*P* Value†	Difference in No. of Tract Fibers*	*P* Value‡
Right corticospinal tract§	0.87 ± 0.15	<.001	27 ± 12	.008
Left corticospinal tract	1.32 ± 0.21	<.001	70 ± 9.2	<.001
Right superior longitudinal fasciculus	0.52 ± 0.16	.005	192 ± 57	.001
Left superior longitudinal fasciculus	0.03 ± 0.14	NS	65 ± 34	.02
Corpus callosum	0.34 ± 0.12	.01	220 ± 149	NS
Right fornix	0.35 ± 0.16	.04	...	...
Left fornix	0.19 ± 0.15	NS	...	...
Left and right fornices	...	...	14 ± 5.5	.02

Note.—NS = not significant.

* Data are mean difference values ± standard deviations.

† *P* values for difference in depiction scores at 1.5- versus 3.0-T tractography.

‡ *P* values for difference in numbers of tract fibers at 1.5- versus 3.0-T tractography.

§ The mean asymmetry index for the corticospinal tract was 0.47 ± 0.11 (standard deviation), and the difference in corticospinal tract asymmetry index at 1.5- versus 3.0-T tractography was significant ($P < .001$).

For corpus callosum tractography, tract depiction scores were better at 3.0 T than at 1.5 T but the numbers of tract fibers did not differ significantly. At corpus callosum tractography, the crossing-fiber problem of unidirectional tracking models (37) may contribute to the discrepancies observed between depiction scores and tract fiber numbers. Corpus callosum tractography is susceptible to the crossing-fiber problem at the centrum semiovale. In this area, a small number of callosal fibers intersect a large number of corticospinal tract fibers. Thus, corpus callosum tractography might reveal a smaller number of fibers than the appropriate fiber trajectory owing to limitations related to the crossing-fiber problem, and differences between 3.0- and 1.5-T imaging may be underestimated.

The statistical methods used may have been responsible for the differences in results obtained at analyses of the depiction scores and the numbers of tract fibers. Although mean differences in the numbers of depicted fibers between 3.0- and 1.5-T imaging were as large as 220, no significant difference was noted. This was probably because of the relatively large numbers of depicted fibers (mean numbers: 3784 at 3.0 T and 3565 at 1.5 T). Low statistical power also may have contributed to this lack of a significant difference.

Depiction scores for right fornix tractography were significantly better at 3.0 T than at 1.5 T, but no significant differences were noted for the left fornix. The numbers of tract fibers depicted at 3.0-T fornix tractography were significantly higher than the numbers depicted at 1.5-T tractography. This result was probably due to the relatively lower volume of limbic fibers compared with the volumes of other fiber bundles. Our DT imaging voxel size was 1.7 × 1.7 × 3.0 mm. The body and crus of the fornix are composed of narrow fiber bundles—they are smaller in diameter than a single voxel—so partial volume-averaging artifacts would have had a greater effect in this region than in the other fiber tracts.

The present study had some limitations. First, the imaging parameters for 3.0-T imaging were not optimized to achieve the best DT image quality. For the most part, we used identical imaging parameters to perform 3.0- and 1.5-T imaging for comparisons so that features other than magnetic field strength would be equivalent. However, differences in T1 and T2* interfere with the equal conditions between 3.0- and 1.5-T imaging. A DT imaging sequence optimized for 1.5-T imaging is not the optimal sequence for 3.0-T imaging. The differences in bandwidth between 3.0- and 1.5-T imaging also may have biased

our results. We tried to keep other acquisition parameters equivalent between 3.0- and 1.5-T imaging, but the bandwidth was higher at 3.0 T. Higher bandwidth results in a reduced signal-to-noise ratio and reduced image distortion. DT imaging at 3.0 T yields a higher signal-to-noise ratio and causes greater magnet susceptibility artifacts owing to the higher static magnetic field strength. We adjusted parameters so that we could use a bandwidth of 1502 Hz per pixel for 3.0-T imaging, which is up to 50% higher than the bandwidth used for 1.5-T imaging. Further optimization of 3.0-T imaging to improve the quality of DT images may be required in the future.

Second, the development of imaging methods to reduce the effects of the crossing-fiber problem, such as high angular DT imaging with high *b* values (38) and diffusion-spectrum imaging (36), is progressing. Other fiber-tracking methods, such as probabilistic tractography to estimate the probability of fiber connections through the data field (39), also are advancing. These advanced methods will affect the results of both 3.0-T and 1.5-T tractography.

In conclusion, DT tractography at 3.0 T enables improved visualization of the corticospinal tract compared with DT tractography at 1.5 T, and 3.0-T tractography of the superior longitudinal fasciculus, corpus callosum, and fornix has some advantages over 1.5-T tractography. Advances in efficient MR sequences are needed to improve the image quality and reliability of 3.0-T DT tractography.

References

1. Basser PJ, Mattiello J, LeBihan D. MR diffusion tensor spectroscopy and imaging. Biophys J 1994;66:259–267.
2. Beaulieu C. The basis of anisotropic water diffusion in the nervous system: a technical review. NMR Biomed 2002;15:435–455.
3. Chenevert TL, Brunberg JA, Pipe JG. Anisotropic diffusion in human white matter: demonstration with MR techniques in vivo. Radiology 1990;177:401–405.
4. Pierpaoli C, Jezzard P, Basser PJ, Barnett A, Di Chiro G. Diffusion tensor MR imaging of the human brain. Radiology 1996;201:637–648.
5. Basser PJ, Pajevic S, Pierpaoli C, Duda J, Aldroubi A. In vivo fiber tractography using DT-MRI data. Magn Reson Med 2000;44:625–632.
6. Mori S, van Zijl PC. Fiber tracking: principles and strategies—a technical review. NMR Biomed 2002;15:468–480.
7. Masutani Y, Aoki S, Abe O, Hayashi N, Otomo K. MR diffusion tensor imaging: recent advance and new techniques for diffusion tensor visualization. Eur J Radiol 2003;46:53–66.
8. Dong Q, Welsh RC, Chenevert TL, et al. Clinical applications of diffusion tensor imaging. J Magn Reson Imaging 2004;19:6–18.
9. Stieltjes B, Kaufmann WE, van Zijl PC, et al. Diffusion tensor imaging and axonal tracking in the human brainstem. Neuroimage 2001;14:723–735.
10. Wakana S, Jiang H, Nagae-Poetscher LM, van Zijl PC, Mori S. Fiber tract-based atlas of human white matter anatomy. Radiology 2004;230:77–87.
11. Clark CA, Barrick TR, Murphy MM, Bell BA. White matter fiber tracking in patients with space-occupying lesions of the brain: a new technique for neurosurgical planning? Neuroimage 2003;20:1601–1608.
12. Yamada K, Kizu O, Mori S, et al. Brain fiber tracking with clinically feasible diffusion-tensor MR imaging: initial experience. Radiology 2003;227:295–301.
13. Huisman TA, Schwamm LH, Schaefer PW, et al. Diffusion tensor imaging as potential biomarker of white matter injury in diffuse axonal injury. AJNR Am J Neuroradiol 2004;25:370–376.
14. Glenn OA, Henry RG, Berman JI, et al. DTI-based three-dimensional tractography detects differences in the pyramidal tracts of infants and children with congenital hemiparesis. J Magn Reson Imaging 2003;18:641–648.
15. Kunimatsu A, Aoki S, Masutani Y, Abe O, Mori H, Ohtomo K. Three-dimensional white matter tractography by diffusion tensor imaging in ischaemic stroke involving the corticospinal tract. Neuroradiology 2003;45:532–535.
16. Tanenbaum LN. 3-T MR imaging: ready for clinical practice [letter]. AJNR Am J Neuroradiol 2004;25:1626–1627.
17. Zhai G, Lin W, Wilber KP, Gerig G, Gilmore JH. Comparisons of regional white matter diffusion in healthy neonates and adults performed with a 3.0-T head-only MR imaging unit. Radiology 2003;229:673–681.
18. Sodickson DK, Manning WJ. Simultaneous acquisition of spatial harmonics (SMASH): fast imaging with radiofrequency coil arrays. Magn Reson Med 1997;38:591–603.
19. Pruessmann KP, Weiger M, Scheidegger MB, Boesiger P. SENSE: sensitivity encoding for fast MRI. Magn Reson Med 1999;42:952–962.
20. Griswold MA, Jakob PM, Heidemann RM, et al. Generalized autocalibrating partially parallel acquisitions (GRAPPA). Magn Reson Med 2002;47:1202–1210.
21. van den Brink JS, Watanabe Y, Kuhl CK, et al. Implications of SENSE MR in routine clinical practice. Eur J Radiol 2003;46:3–27.
22. Jaermann T, Crelier G, Pruessmann KP, et al. SENSE-DTI at 3 T. Magn Reson Med 2004;51:230–236.
23. Naganawa S, Koshikawa T, Kawai H, et al. Optimization of diffusion-tensor MR imaging data acquisition parameters for brain fiber tracking using parallel imaging at 3 T. Eur Radiol 2004;14:234–238.
24. Nagae-Poetscher LM, Jiang H, Wakana S, Golay X, van Zijl PC, Mori S. High-resolution diffusion tensor imaging of the brain stem at 3 T. AJNR Am J Neuroradiol 2004;25:1325–1330.
25. Bastin ME, Armitage PA. On the use of water phantom images to calibrate and correct eddy current induced artefacts in MR diffusion tensor imaging. Magn Reson Imaging 2000;18:681–687.
26. Pajevic S, Pierpaoli C. Color schemes to represent the orientation of anisotropic tissues from diffusion tensor data: application to white matter fiber tract mapping in the human brain. Magn Reson Med 1999;42:526–540.
27. Naidich TP, Valavanis AG, Kubik S. Anatomic relationships along the low-middle convexity. I. Normal specimens and magnetic resonance imaging. Neurosurgery 1995;36:517–532.
28. Mori S, Kaufmann WE, Davatzikos C, et al. Imaging cortical association tracts in the human brain using diffusion-tensor-based axonal tracking. Magn Reson Med 2002;47:215–223.
29. Lazar M, Field AS, Lee J, et al. Lateral asymmetry of superior longitudinal fasciculus: a white matter tractography study (abstr). In: Proceedings of the 12th Meeting of the International Society for Magnetic Resonance in Medicine. Berkeley, Calif: International Society for Magnetic Resonance in Medicine, 2004; 1290.

30. Fera F, Yongbi MN, van Gelderen P, Frank JA, Mattay VS, Duyn JH. EPI-BOLD fMRI of human motor cortex at 1.5 T and 3.0 T: sensitivity dependence on echo time and acquisition bandwidth. J Magn Reson Imaging 2004;19:19–26.

31. Willinek WA, Born M, Simon B, et al. Time-of-flight MR angiography: comparison of 3.0-T imaging and 1.5-T imaging—initial experience. Radiology 2003;229:913–920.

32. Willinek WA GJ, von Falkenhausen M, et al. 3.0T contrast-enhanced, submillimeter MRA of the supraaortic arteries: does the signal gain at high field strength allow to replace the phased array coil by the quadrature body coil? (abstr). In: Proceedings of the 12th Meeting of the International Society for Magnetic Resonance in Medicine. Berkeley, Calif: International Society for Magnetic Resonance in Medicine; 2004: 1523.

33. Graf H, Schick F, Claussen CD, Seemann MD. MR visualization of the inner ear structures: comparison of 1.5 Tesla and 3 Tesla images. Rofo 2004;176:17–20.

34. Hunsche S, Moseley ME, Stoeter P, Hedehus M. Diffusion-tensor MR imaging at 1.5 and 3.0 T: initial observations. Radiology 2001; 221:550–556.

35. Yagishita A, Nakano I, Oda M, Hirano A. Location of the corticospinal tract in the internal capsule at MR imaging. Radiology 1994;191:455–460.

36. Lin CP, Wedeen VJ, Chen JH, Yao C, Tseng WY. Validation of diffusion spectrum magnetic resonance imaging with manganese-enhanced rat optic tracts and ex vivo phantoms. Neuroimage 2003;19:482–495.

37. Wiegell MR, Larsson HB, Wedeen VJ. Fiber crossing in human brain depicted with diffusion tensor MR imaging. Radiology 2000; 217:897–903.

38. Tuch DS, Reese TG, Wiegell MR, Makris N, Belliveau JW, Wedeen VJ. High angular resolution diffusion imaging reveals intravoxel white matter fiber heterogeneity. Magn Reson Med 2002;48:577–582.

39. Behrens TE, Woolrich MW, Jenkinson M, et al. Characterization and propagation of uncertainty in diffusion-weighted MR imaging. Magn Reson Med 2003;50:1077–1088.